Journal of Environmental Radioactivity 137 (2014) 88–95

Contents lists available at ScienceDirect

Journal of Environmental Radioactivity

journal homepage: www.elsevier.com/locate/jenvrad

When the dust settles: stable xenon isotope constraints on the formation of nuclear fallout

W.S. Cassata [a, *], S.G. Prussin [b], K.B. Knight [a], I.D. Hutcheon [a], B.H. Isselhardt [a], P.R. Renne [c, d]

[a] Lawrence Livermore National Laboratory, 7000 East Avenue, Livermore, CA 94550, USA
[b] Department of Nuclear Engineering, University of California – Berkeley, 4113 Etcheverry Hall MC 1730, Berkeley, CA 94720-1730, USA
[c] Berkeley Geochronology Center, 2455 Ridge Road, Berkeley, CA 94709, USA
[d] Department of Earth and Planetary Sciences, University of California – Berkeley, 307 McCone Hall MC 4767, Berkeley, CA 94720-4767, USA

ARTICLE INFO

Article history:
Received 24 December 2013
Received in revised form
5 May 2014
Accepted 9 June 2014
Available online 9 July 2014

Keywords:
Nuclear fallout
Xenon
Fission product
Chemical fractionation
Nuclear fireball

ABSTRACT

Nuclear weapons represent one of the most immediate threats of mass destruction. In the event that a procured or developed nuclear weapon is detonated in a populated metropolitan area, timely and accurate nuclear forensic analysis and fallout modeling would be needed to support attribution efforts and hazard assessments. Here we demonstrate that fissiogenic xenon isotopes retained in radioactive fallout generated by a nuclear explosion provide unique constraints on (1) the timescale of fallout formation, (2) chemical fractionation that occurs when fission products and nuclear fuel are incorporated into fallout, and (3) the speciation of fission products in the fireball. Our data suggest that, in near surface nuclear tests, the presence of a significant quantity of metal in a device assembly, combined with a short time allowed for mixing with the ambient atmosphere (seconds), may prevent complete oxidation of fission products prior to their incorporation into fallout. Xenon isotopes thus provide a window into the chemical composition of the fireball in the seconds that follow a nuclear explosion, thereby improving our understanding of the physical and thermo-chemical conditions under which fallout forms.

© 2014 Elsevier Ltd. All rights reserved.

1. Introduction

With the Cold War almost a quarter-century past and non-proliferation efforts accelerating, nuclear weapons will hopefully never be used again. In the unfortunate event that a nuclear weapon was detonated in a metropolitan area, nuclear forensic analysis and fallout modeling would be critically important to the decision-making process that followed. Chemical and isotopic analyses of radioactive fallout generated during a nuclear explosion may aid in attributing an attack to a state or non-state actor and in assessing the likelihood that additional weapons exist (Fahey et al., 2010; Joint Working Group of the American Physical Society and the American Association for the Advancement of Science, 2010; National Research Council of the National Academies – Committee on Nuclear Forensics, 2010). Fallout modeling provides predictions of the geographic distribution of hazardous radionuclides, and is also an important component of hazard assessments. Given the complexity of fallout debris formation, placing constraints on variables such as the time and temperatures of formation and the relative volatilities of condensing species in the fireball can aid in the development of a realistic dynamical model for the overall process. Such constraints on the physico-chemical conditions under which fallout forms and device components become incorporated within the fireball are fundamental to models of the transport of fission products in fallout (e.g., Beck et al., 2010; Freiling, 1961), and may improve their predictive power.

Following a near-surface nuclear explosion, fallout particles and surface melt glass are generated in the vicinity of ground zero. Proximal fallout particles occur as nm- to cm-sized, irregularly-shaped to aerodynamically-shaped (i.e., spherical-, ovoidal-, and dumbbell-shaped) glass beads that are morphologically similar to tektites and lunar impact spherules (Fig. 1; e.g., Eby et al., 2010). They are generally composed of transparent, colorless to pale yellow, green, or black glass, and contain variable concentrations of vesicles (e.g., Adams et al., 1960). Individual fallout glasses exhibit a diversity of macro- and micro-scopic textural characteristics, from compositional homogeneity to heterogeneous mixtures of unmelted surface materials with glasses of different compositions. Fallout particles are formed when molten or partially molten

* Corresponding author. Tel.: +1 925 423 2812.
E-mail address: cassata2@llnl.gov (W.S. Cassata).

http://dx.doi.org/10.1016/j.jenvrad.2014.06.011
0265-931X/© 2014 Elsevier Ltd. All rights reserved.

Fig. 1. Optical microscope images of the analyzed fallout particles.

surface materials are entrained in the hot, radioactive fireball, where they interact with condensing bomb, fission, and surface materials that were vaporized by the explosion (Adams et al., 1960; Izrael, 2002). The resulting melt glasses contain constituents of the device (metals, explosives, unfissioned fuel, etc.), fission and activation products generated during the explosion, and components of the surrounding earth and buildings (e.g., Belloni et al., 2011; Bellucci and Simonetti, 2012; Bellucci et al., 2013a, 2013b; Parekh et al., 2006; Pittauerova et al., 2010).

Previous investigations of fallout have employed inductively coupled plasma mass spectrometry (ICP-MS) to determine the isotopic composition of actinides (Bellucci et al., 2013a), alpha, beta, and gamma spectroscopy to determine fission product abundances (e.g., Atkatz and Bragg, 1995; Belloni et al., 2011; Bellucci et al., 2013b; Mackin et al., 1960; Parekh et al., 2006; Pittauerova et al., 2010; Schlauf et al., 1997), autoradiography to determine radionuclide distributions (e.g., Adams et al., 1960; Belloni et al., 2011; Fahey et al., 2010), secondary and transmission electron microscopy and electron probe microanalysis to determine spatial distributions of elements and weapon components (Bellucci and Simonetti, 2012; Bunch et al., 2012; Eby et al., 2010; Fahey et al., 2010), and secondary ion mass spectrometry to identify spatial variations in the isotopic composition of U and Pu (Fahey et al., 2010). To date, there are only two publicly available measurements of stable noble gas concentrations in radioactive debris, both of which are from glasses created during the Trinity test (Jessberger et al., 1992; Meshik et al., 2005). Despite the paucity of available data, noble gas analysis represents a rapid, non-destructive approach to constraining the time of debris formation and the magnitude of chemical fractionation (processes that change the relative abundances of species during their incorporation into fallout) that attends condensation in the fireball. These constraints are the focus of the present study.

Xenon isotopes are ideal for studying the formation of glassy debris following a nuclear explosion as its heavy nuclides are stable, terminal fission products in the mass chains 131, 132, 134, and 136, each of which represents more than ~4% of the total number of fissions (England and Rider, 1994; Tables S1 and S2). Given the volatility and negligible solubility of Xe in silicate melts at high temperatures (Shibata and Takahashi, 1998), both atmospheric and fissiogenic Xe are effectively excluded from fallout during its formation. Fissiogenic Xe isotopes contained in glassy fallout thus reflect post-formation ingrowth from the decay of the less volatile precursors tin (Sn), antimony (Sb), tellurium (Te), and iodine (I). Because the precursor nuclides have diverse chemical characteristics and short half-lives (seconds to tens of seconds for the rapidly-decaying nuclides), the isotopic composition of Xe preserved in debris reflects both the relative volatilities of the precursor nuclides and the time at which the surface of the molten debris becomes impervious to mass transfer.

This paper presents an analysis of the stable Xe isotope composition in glassy fallout formed during the explosion of a Pu-fueled device. The data reported are used to address the following questions: What is the time range over which fissiogenic nuclides, unfissioned fuel, and materials from the device are incorporated into melts within the fireball? How are fissiogenic nuclides in the mass chains 131–136 chemically fractionated from each other during the formation of mm-sized glassy fallout particles (i.e., what are the relative volatilities of the precursor nuclides)? What are the implications of such fractionation trends for understanding the chemical and thermodynamic conditions that prevailed in the nuclear fireball (i.e., was it reducing, oxidizing, etc.)? What can be said about the mechanisms (i.e., the physical processes) by which fallout is formed based on the thermal, temporal, and chemical constraints gleaned from the Xe isotope data?

2. Materials, methods, and results

Several kilograms of sediment containing debris and glass were collected at a distance of ~1 km from the ground zero of a historical, near surface test of a Pu-fueled device. The sediment sample was washed to remove dust and then sieved into discrete size fractions. Individual, glassy fallout particles for this study were hand-picked from the 1–2 mm size fraction and imaged under a binocular microscope (Fig. 1). The quasi-spherical specimens were then placed under ultra-high vacuum and incrementally heated in four steps of increasing power (corresponding to temperatures of ~600–1600 °C) using a 50 W CO_2 laser. The released gas was purified using two SAES getters (one hot and one cold), analyzed using a Mass Analyzer Products 215-50 mass spectrometer, and measured statically on a Balzers SEV-217 electron multiplier. Isotope abundances were calculated as peak intensities at the time of gas admission to the mass spectrometer and were determined by polynomial (first to third order) regressions to peak hopping scans through four to twenty cycles.

Measured abundances of fissiogenic Xe isotopes were corrected for system backgrounds, atmospheric contributions, and spectrometer mass discrimination. Background corrections were applied to account for Xe that passively outgasses from stainless steel components of the processing line when operated in static vacuum mode during sample analysis. These system backgrounds were measured before and after each sample using the same

Table 1
Xenon isotope data.

#	Power (W)	$^{132}Xe_f$ F	$^{132}Xe_f$ (%)	$^{131}Xe/^{132}Xe \pm 1\sigma$	$^{131}Xe/^{134}Xe \pm 1\sigma$	$^{131}Xe/^{136}Xe \pm 1\sigma$	$^{132}Xe/^{134}Xe \pm 1\sigma$	$^{132}Xe/^{136}Xe \pm 1\sigma$	$^{134}Xe/^{136}Xe \pm 1\sigma$
Debris A									
1	15 W	0.278	99.9	1.157 ± 0.048	3.400 ± 0.140	31.124 ± 1.389	2.939 ± 0.121	26.902 ± 1.196	9.153 ± 0.407
2	20 W	0.411	99.9	1.138 ± 0.048	3.061 ± 0.128	29.396 ± 1.366	2.691 ± 0.114	25.842 ± 1.211	9.603 ± 0.449
3	30 W	0.727	100.0	1.128 ± 0.048	2.971 ± 0.122	27.437 ± 1.197	2.634 ± 0.112	24.327 ± 1.094	9.235 ± 0.407
4	35 W	1.000	99.9	1.094 ± 0.045	2.579 ± 0.108	24.476 ± 1.019	2.357 ± 0.098	22.369 ± 0.931	9.490 ± 0.400
		Weighted average:		1.128 ± 0.024	2.946 ± 0.271	24.478 ± 2.335	2.624 ± 0.193	24.497 ± 1.624	9.361 ± 0.207
Debris B									
1	15 W	0.039	80.5	1.406 ± 0.083	8.389 ± 0.781	59.767 ± 19.708	5.968 ± 0.553	42.515 ± 14.015	7.124 ± 2.403
2	20 W	0.307	99.7	1.273 ± 0.055	7.668 ± 0.334	n/a ± n/a	6.023 ± 0.262	n/a ± n/a	n/a ± n/a
3	25 W	0.597	100.0	1.222 ± 0.052	6.834 ± 0.308	56.285 ± 3.542	5.590 ± 0.251	46.042 ± 2.891	8.236 ± 0.533
4	35 W	1.000	99.7	1.278 ± 0.064	7.188 ± 0.358	60.829 ± 3.436	5.626 ± 0.279	47.608 ± 2.679	8.462 ± 0.477
		Weighted average:		1.274 ± 0.030	7.276 ± 0.186	58.644 ± 2.447	5.762 ± 0.147	46.800 ± 1.946	8.335 ± 0.351
Debris C									
1	15 W	0.270	90.7	1.164 ± 0.055	3.026 ± 0.156	39.475 ± 9.205	2.599 ± 0.138	33.902 ± 7.915	13.046 ± 3.057
2	20 W	0.569	98.8	1.114 ± 0.060	2.776 ± 0.149	27.226 ± 1.513	2.493 ± 0.134	24.448 ± 1.353	9.807 ± 0.544
3	30 W	0.960	99.8	1.111 ± 0.045	2.761 ± 0.116	29.306 ± 1.314	2.486 ± 0.104	26.389 ± 1.178	10.615 ± 0.485
4	35 W	1.000	97.2	1.164 ± 0.055	3.099 ± 0.157	32.537 ± 3.776	2.663 ± 0.133	27.962 ± 3.239	10.500 ± 1.230
		Weighted average:		1.136 ± 0.027	2.887 ± 0.071	28.794 ± 0.954	2.549 ± 0.062	25.815 ± 0.852	10.312 ± 0.345

Isotope ratios were corrected for extraction line backgrounds, detector baseline, spectrometer discrimination, and atmospheric contributions.
Uncertainties reflect the analytical uncertainties on isotope measurements, backgrounds, and mass discrimination determinations.
$^{132}Xe_f$ F is the cumulative fraction of fissionogenic ^{132}Xe released.
$^{132}Xe_f$ % is the percent of the total ^{132}Xe in a given extraction that is fissionogenic (the remainder is atmospheric).
n/a indicates that ^{136}Xe was not measured.

analytical procedure employed during fallout analyses, but without firing the laser. The bracketing background measurements were averaged and then subtracted from the measured isotope abundances of the fallout analyses. Atmospheric corrections were applied to account for non-fissiogenic ^{131}Xe, ^{132}Xe, ^{134}Xe, and ^{136}Xe trapped within the samples. This correction is made assuming that the non-fissiogenic Xe has an atmospheric isotopic composition. ^{129}Xe and ^{130}Xe (non-fissiogenic isotopes derived solely from trapped atmospheric gas) are measured along with the fissiogenic isotopes, and a proportional amount of ^{131}Xe, ^{132}Xe, ^{134}Xe, and ^{136}Xe is subtracted from the measured isotope abundances. The discrimination correction is applied to account for instrumental mass biases in detector and ionization efficiency. The instrumental mass discrimination (1.0008 ± 0.0030 per atomic mass unit) was determined from analyses of atmospheric Xe aliquots delivered from a pipette system, interspersed with the unknowns. More detailed descriptions of the application of atmospheric and discrimination corrections to noble gas mass spectrometry measurements are given in Renne et al. (2009).

Complete analytical results, corrected for backgrounds, atmospheric contributions, and spectrometer mass discrimination, are given in Table 1. Background corrections were generally <0.1% of the fissiogenic Xe isotope abundances. Incompletely degassed atmospheric Xe contained within the fallout typically comprised <1% of the total Xe (Table 1). The magnitude of the uncertainty on a given Xe isotope ratio primarily reflects the signal sizes, which are generally smallest in the first, low-temperature gas extractions. Although inter-sample variations exist, the isotopic compositions of Xe in each of the four extractions of increasing laser power used to degas individual samples were statistically indistinguishable. As such, weighted average Xe isotope ratios were used in all calculations discussed below. The isotopic composition of fissionogenic Xe in the fallout is not equivalent to that expected from the cumulative yields of the decay chains, which indicates that chemical fractionation (i.e., the selective incorporation of fission product precursors of a given element or elements) occurred during the fallout formation. In the following section we explore the effects of different precursor volatility relationships on Xe isotope ratios.

3. Calculations and data discussion

The relative abundance of any fission product following the nearly instantaneous fission in a nuclear detonation varies in time according to its independent fission yield[1] and those of its precursors in a mass chain, its β-decay half-life and those of its precursors, and the proportions of fissions that occurred in the various fuel isotopes that underwent fission. Radioactive fission products have half-lives typically in the range of about 50 ms to 10^5 y, and eventually all decay to a stable, terminal isotope of the same mass number – the highest-Z member of a β-decay chain.[2] As a fireball cools in the seconds following a nuclear detonation, fission-product nuclides will form atoms and compounds by collisional mechanisms. They will agglomerate and condense onto the surfaces of any molten detritus from the area immediately surrounding ground zero at a rate dependent on their concentrations and the temperature dependence of the various chemical forms in which they may exist. Those forms that are more refractory will tend to concentrate in the liquids or melts present in the fireball earlier than those in more volatile forms, resulting in chemical fractionation. Thus the measured ratio of two terminal fissiogenic nuclides depends on the time at which the surface of the molten silicate solidifies to glass and the time-integrated relative volatilities of the chemical forms of the precursor nuclides with respect to the molten surfaces onto which they condense and are incorporated.

^{131}Xe, ^{132}Xe, ^{134}Xe, and ^{136}Xe are the stable, terminal nuclides to which short-lived fission products in their respective decay chains transmute in the general order Sn → Sb → Te → I → Xe (Fig. 2). In the absence of chemical fractionation and radioactive decay, the relative abundance of an isotope of Xe generated by a device fueled with ^{239}Pu, ^{240}Pu, and ^{241}Pu is given by the sum of the independent

[1] The independent fission yield of a fission product is the yield produced following fission and the emission of prompt fission neutrons.

[2] Although the majority of radioactive fission products decay by β-emission and thus preserve a mass number, A, there are a few very short-lived nuclides that decay by β-delayed neutron emission and thus contribute to the yield of the mass chain A − 1 (see Fig. 2).

yields I_p of all fission products p in the ^{13X}Xe decay chain, each weighted by the fraction F_p^{13X} of that nuclide decay series that ends at the stable isotope of Xe[3], according to the following expression:

$$N_{Xe}^{13X} = \sum_p \left(I_p^{Pu}\right)\left(F_p^{13X}\right), \quad (1)$$

where I_p^{Pu} is given by

$$I_p^{Pu} = \frac{\left(I_p^{239}\right)(\sigma_F^{239})(f^{239}) + \left(I_p^{240}\right)(\sigma_F^{240})(f^{240}) + \left(I_p^{241}\right)(\sigma_F^{241})(f^{241})}{(\sigma_F^{239})(f^{239}) + (\sigma_F^{240})(f^{240}) + (\sigma_F^{241})(f^{241})}, \quad (2)$$

and f is the atom fraction of a given fuel isotope (Table S1), σ is the fission cross section of a given fuel isotope (Table S1), and I_p^x is the isotope-specific independent yield (England and Rider, 1994; Table S2). As discussed above, the isotopic composition of fissiogenic Xe in fallout (Table 1) is not equivalent to the cumulative yields of the decay chains (see Table S2). Discrepancies arise because nuclides in the decay chains, the relative abundances of which vary over time due to radioactive decay, are chemically fractionated during the condensation/deposition process. While the relative volatilities of fission products are mass-independent (because fractionation is a chemical process), the chemical transmutation of fission products due to decay in the fireball differentially affects the isotopes, and is most prominent in the higher mass decay chains (Fig. 2). As such, Xe isotope ratios involving ^{136}Xe are particularly sensitive to the time at which fallout interacts with fission products in the fireball, while those involving lower mass Xe isotopes are sensitive to chemical fraction during the condensation/deposition process (discussed in more detail below). It will be shown in the following sections that there are a sufficient number of Xe isotopes with which to uniquely constrain both chemical fractionation and the timescale of interaction.

In the absence of a detailed model of the time-dependent temperatures and chemistries of the various precursor nuclides, we follow a simplified approach to constraining fractionation wherein we define the "refractory yield" R_{Xe}^{13X} of a given Xe isotope in the glassy debris as the sum of the independent yields of the precursor nuclides in the mass chain, each adjusted for radioactive decay to the time t at which mass transport across the surface of the glass is effectively ended and weighted by their relative apparent volatilities, as

$$R_{Xe}^{13X}(t) = \sum_p \left[N_p^{13X}(t)\right]\left(F_p^{13X}\right)(1 - V_p), \quad (3)$$

where $N_p^{13X}(t)$ is the number of atoms of the fission product at time t determined by solving Bateman equations [assuming the isotopic composition of fireball at t_o is given by the independent yield distribution for fission of Pu by fission-spectrum neutrons (Eq. (2); Table S1 and S2)], F_p^{13X} is as defined above, and V_p [the effective relative volatility of the fission product with respect to the most refractory precursor in the decay chain (in this case Sn)] varies between 0 (not fractionated) and 1 (completely fractionated – unable to condense). Given its volatility, any Xe present in fallout can confidently be considered an *in situ* decay product of its precursor nuclides, and not a primary condensate. This assumption implies that the fissiogenic Xe isotopes in the glassy fallout are proxies for the incorporation of the less volatile fission products Sn, Sb, Te, and I, and do not reflect the isotopic composition of Xe in the fireball. In the absence of knowledge of appropriate V_p values, here we compare the measured Xe isotope ratios with those predicted for different relative volatility relationships (i.e., different hypothetical chemical fractionation scenarios) in order to constrain them.

Let us begin with the assumption that Sn, Sb, Te, and I are not fractionated relative to each other during the condensation process (i.e., $V_p = 0$ for each element). Because the half-lives of the I isotopes in the mass chains of interest (minutes to hours) are very long compared to the timescales over which the fireball cools (seconds; see below), to a good approximation I does not decay to volatile (non-condensing) Xe prior to the termination of mass transfer across the surface of the glass. Thus the refractory yield of a Xe isotope will simply reflect the sum of the independent yields of its precursors (Table S2), and without chemical fractionation during the condensation process the ratio of the abundances of any two Xe isotopes produced by the *in situ* decay of Sn, Sb, Te, and I would not be time-dependent. By comparison with the measured ratios obtained from fallout (Table 1) it is clear that such a simple model does not adequately account for the experimental data.

Now assume that both I and Xe are completely volatile ($V_p = 1$), but Sn, Sb, and Te are incorporated and not fractionated relative to each other during the condensation process ($V_p = 0$). In this case, the extent to which Te decays to I prior to solidification of the surface of the molten silicate droplets determines the Xe isotope abundances in fallout. The half-lives of precursor isotopes ^{131}Te, ^{132}Te, and ^{134}Te are orders of magnitude longer than the timescales over which the fireball cools. Thus the ratio of the abundances of any two of these Xe isotopes (mass chains A = 131, 132, and 134) would be time-independent (denoted by the white circle labeled "Sn, Sb, Te not fractionated" in Fig. 3a). In contrast, the 17.6-second half-life of ^{136}Te is sufficiently short such that significant radioactive decay can take place on the timescale of a few seconds. For this mass chain, the sum of the condensable precursor yields would vary with time, and the measured ratio of ^{136}Xe to ^{131}Xe, ^{132}Xe, and ^{134}Xe would exhibit significant variation depending on the time at which the melt solidifies (see gray-scale circles labeled "Sn, Sb, Te not fractionated" in Fig. 3b). Regardless, the experimental data shown in Fig. 3 are not consistent with Sn, Sb, and Te condensing in an unfractionated manner.

Finally, assume that Te, in addition to I and Xe, is completely volatile ($V_p = 1$), such that only Sn and Sb are incorporated and not fractionated relative to each other during the condensation process ($V_p = 0$). In this scenario, the extent to which Sb decays to volatile (non-condensing) Te prior to the silicate melt surfaces solidifying determines the Xe isotope ratios in fallout. The half-lives of the fissiogenic isotopes of Sb range from 23 min to less than a second, leading to significant variations in the abundances of at least some of the condensable precursor nuclides in the seconds following a nuclear explosion. Measured Xe isotope ratios would thus depend on the time at which Sn and Sb condensed (see Fig. 3 and insets). Likewise, significant variations in Xe isotopes ratios would be expected if only Sn is partially refractory (see Fig. 3 and insets). Fig. 3

[3] F_p^{13X} is unity unless the nuclide decays by delayed neutron emission (see Fig. 2).

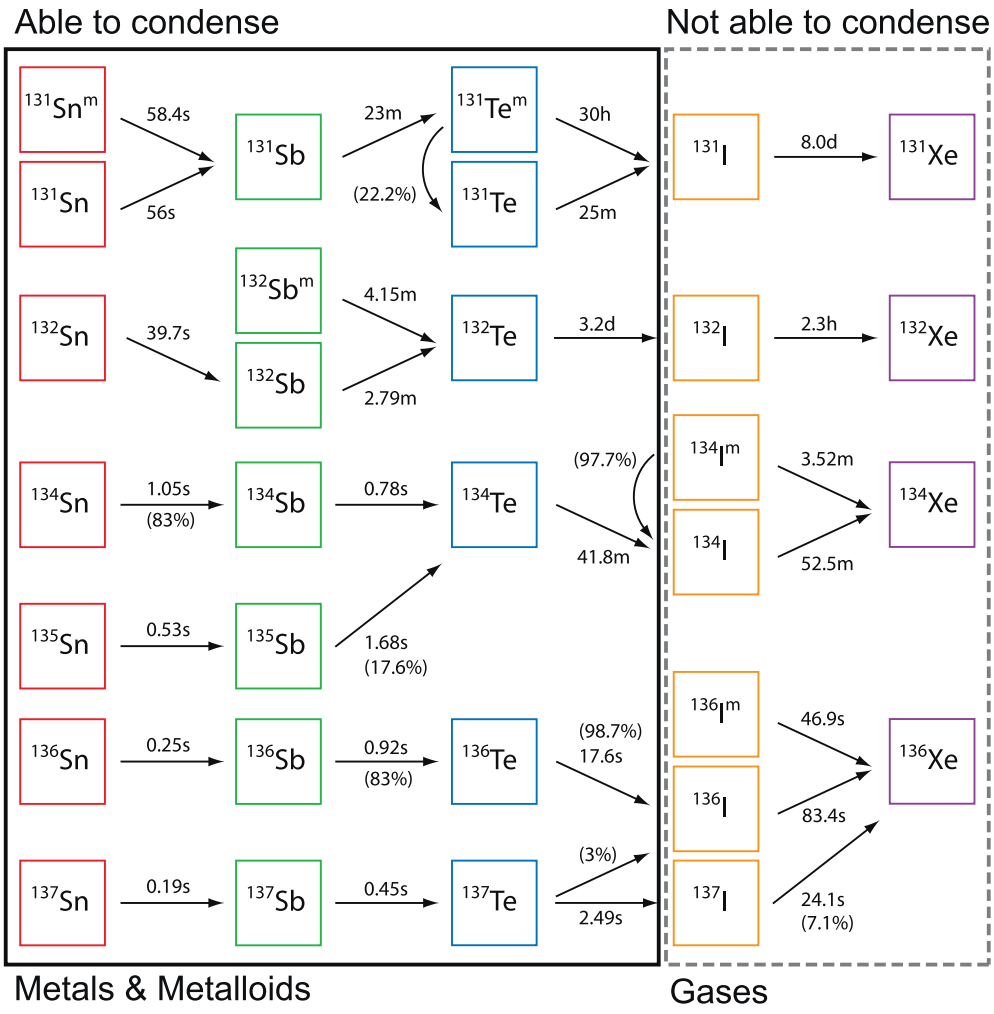

Fig. 2. Radionuclide decay paths used to calculate time-dependent Xe isotope compositions. Branching fractions for nuclides that decay by β-emission and β-delayed neutron emission are given in percentages.

again illustrates that the experimental data are not consistent with Te being completely volatile, or with both Sb and Te being completely volatile.

Having explored simple models wherein fissiogenic nuclides are either completely volatile or unfractionated with respect to Sn without finding a satisfactory fit to the data (Fig. 3), we now consider relative volatilities of the respective fission products. Assume first that I and Xe are completely volatile ($V_p = 1$), Sn and Sb are at least partially refractory and not fractionated from each other ($V_p = 0$), while Te is able to condense but more volatile than Sn and Sb ($0 < V_p < 1$). In this case, for a given incorporation time, data would lie along a line that connects the Xe isotope composition predicted if Sn, Sb, and Te were not fractionated to that predicted if only Sn and Sb were not fractioned (see dashed purple lines in Fig. 3) . The more volatile the behavior of Te relative to Sn and Sb, the closer the data would lie to the latter end-member, and vice versa. If both Sb and Te were equally volatile relative to Sn, then the data would lie along a mixing array connecting the Xe isotope composition predicted if Sn, Sb, and Te were not fractioned with that predicted if only Sn is refractory (see dashed red lines in Fig. 3). If Sb was more volatile than Sn, but more refractory than Te, then the data would lie between the former two linear arrays, the exact position of which would depend on the relative volatilities of Sb and Te. The fact that the measured Xe isotope ratios lie along the dashed purple lines described above (Fig. 3) suggests that Sn and Sb were not fractionated relative to each other ($V_p = 0$), whereas Te was principally volatile ($0 < V_p < 1$). Significant Te volatility has been also observed in previous investigations of nuclear fallout (e.g., Kawahara et al., 1980) and fission products in synthetic nuclear fallout subjected to thermal distillation (e.g., Carney et al., 2014).

4. Constraints on fallout formation

4.1. Time of condensation and magnitude of chemical fractionation

Because each fissiogenic decay chain is characterized by a different independent yield distribution (Table S2) and radionuclide decay timescale (Fig. 2), a sufficient number of independent variables are required to uniquely constrain the time at which radionuclide incorporation ceases (i.e., the time at which the silicate droplet surfaces become impervious to mass transfer) and the extent to which Xe precursors are chemically fractionated. In the present case, the measurement of three fissiogenic Xe isotope ratios permits a unique solution to the time of incorporation and the relative volatilities of Sb and Te with respect to Sn. Our approach to finding the best-fit solutions to these variables is as follows. For each sample we quantified the three independent observations

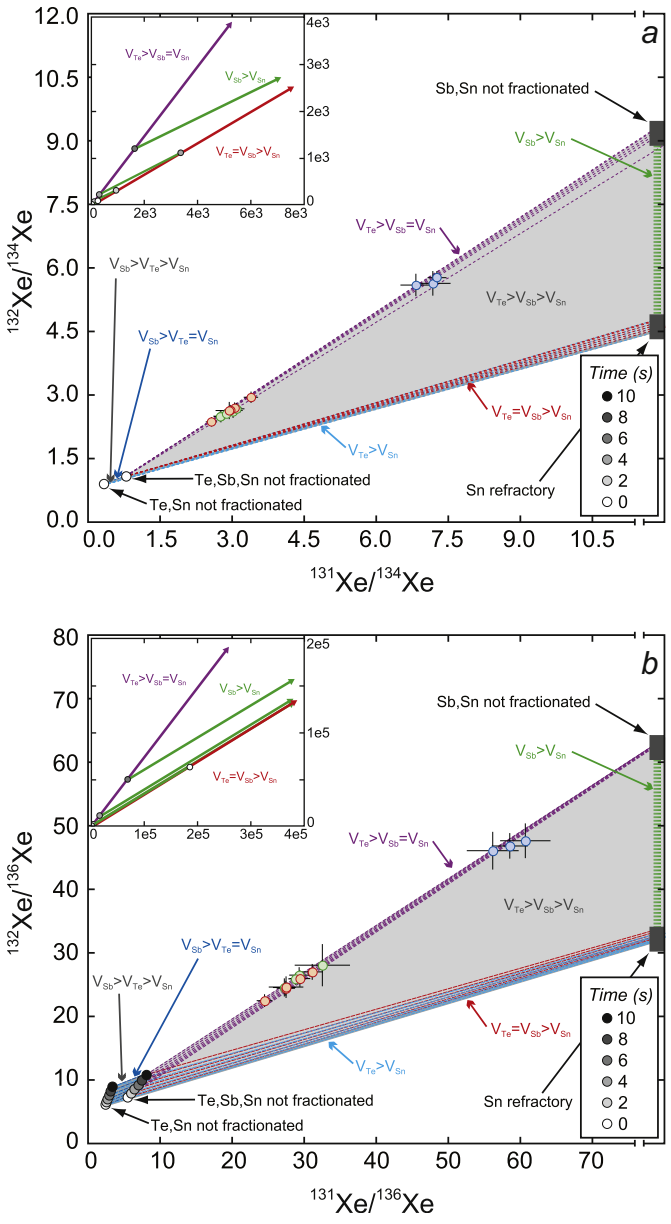

Fig. 3. Xenon three-isotope plots. Individual incremental heating step data and weighted averages are shown with 1σ uncertainties (Debris A – red; Debris B – blue; Debris C – green). Gray-scale circles represent Xe isotopic compositions that would be observed if the indicated species condensed in an unfractionated manner at the time denoted by the legend to the lower, right. Dashed lines connect the time-dependent Xe isotopic compositions predicted for the various end-member fractionation scenarios. Data that lie along these mixing lines are consistent with partial volatility (V) of one or more nuclides relative to the more refractory species, as indicated by V subscripts. Note the change in x-axis scale that precedes the Xe isotope compositions that would be observed if only Sn was refractory or if Sn and Sb condensed in an unfractionated manner. Expected Xe isotope compositions associated with these scenarios lie off the scale of the main figures, and are shown in the insets to the upper, left. Measured isotopic compositions of Xe in fallout debris are consistent with Te being volatile relative to Sn and Sb, which are not fractionated relative to each other. Individual data points with uncertainties that exceeded the weighted average uncertainty by more than 4σ were excluded from the figure to improve its clarity (but were included in weighted average calculations). Models are based on independent yields given in England and Rider (1994), assuming an isotopic composition of Pu-fuel listed in Table S1. (For interpretation of the references to colour in this figure legend, the reader is referred to the web version of this article.)

($^{131}Xe/^{132}Xe$, $^{131}Xe/^{134}Xe$, and $^{131}Xe/^{136}Xe$) by mass spectrometry. We sought best-fit values and uncertainties for the three independent variables to which the observed isotope ratios are related [V_{Te} (the volatility of Te with respect to Sn), V_{Sb} (the volatility of Sb with respect to Sn), and t (the time at which debris ceased to interact with the fireball)] according to the following equation:

$$\frac{^{131}Xe}{^{13X}Xe} = \frac{\sum_p \left[N_p^{131}(t)\right]\left(F_p^{131}\right)(1-V_p)}{\sum_p \left[N_p^{13X}(t)\right]\left(F_p^{13X}\right)(1-V_p)} \quad (4)$$

where all terms are as defined in Section 3. Best-fit values of V_{Te}, V_{Sb}, and t were those that minimized the error-weighted sum-of-squares residuals (represented by the χ^2_υ statistic) between the measured Xe isotope ratios and those predicted by model solutions to Eq. (4), where the three aforementioned variables were systematically varied over all plausible values. We estimated the uncertainty in the best-fit values from the range of solutions for which χ^2_υ was below a critical value obtained from statistics tables. For one degree of freedom, the 1σ error envelope is defined by solutions for which χ^2_υ is 1 unit above that of the best-fit solution (i.e., minimum $\chi^2_\upsilon = 1$; χ^2_υ of 1σ error envelope = 2). The uncertainty estimates reflect measurement error only, and do not include uncertainties on the independent yields and other physical parameters (e.g., branching ratios, decay constants, etc.).

For the three glassy fallout particles studied, best-fit solutions to the system of equations indicate that the times at which mass transfer across their surfaces effectively ended were 0.2 ± 0.4 s, 0.0 ± 0.1 s, and 2.9 ± 1.1 s, with corresponding fractional volatilities of Te and Sb relative to Sn of 0.84 ± 0.01, 0.85 ± 0.01, and 0.93 ± 0.01 and 0.00 ± 0.04, 0.00 ± 0.06, and 0.20 ± 0.16, respectively (Table 2). Interestingly, the particle that interacted with the fireball longer/later than the others (Debris C) is significantly more depleted in Te, which suggests it may have been entrained in the toroid or traversed a more circuitous path in a slower-cooling region of the fireball compared to the other two samples. Those pieces of debris with closure times of <0.5 s may have been ballistically ejected from the fireball at an earlier time or may have obliquely traversed the fireball. Differences in the time at which fallout ceased to interact with fission products may also be related to the time at which the sediment was entrained in the buoyantly rising fireball.

4.2. Thermochemical environment during fallout formation

Models of fallout formation, while comprehensive in principle, contain fairly simple assumptions regarding the thermal and chemical environments involved because of a lack of detailed experimental data and the complexity of the mechanisms proposed (Miller, 1960; Stewart, 1956). The concurrent processes of chemical bonding, radioactive decay, condensation, agglomeration, turbulent flow, and thermal equilibration involved in the formation of fallout are complex and strongly time dependent. It has generally been assumed that the device components and fission products were exposed to a strongly oxidizing environment as atmospheric oxygen was drawn into the fireball soon after detonation (Adams et al., 1960; Adams and O'Connor, 1957; Miller, 1960; Stewart, 1956). The xenon isotope measurements described here may be in disagreement with this assumption.

The data and analysis presented by Narasimhan et al. (2005) suggest that in the presence of sufficient oxygen, Te will most likely be present in the gas phase as TeO_2 and TeO at temperatures on the order of 1400–1600 °C and that the total vapor pressure above TeO_2 (m.p. = 733 °C) would extrapolate to about 1 atm at a temperature of ~1080 °C and would be about 0.01 atm at 867 °C.

Table 2
Time of formation and chemical fractionation constraints.

Sample	Time (s) ± 1σ	V_{Te} ± 1σ	V_{Sb} ± 1σ	χ^2_ν
Debris A	0.2 ± 0.4	0.840 ± 0.010	0.000 ± 0.039	0.69
Debris B	2.9 ± 1.1	0.933 ± 0.011	0.200 ± 0.163	0.07
Debris C	0.0 ± 0.1	0.848 ± 0.007	0.000 ± 0.064	4.07

V_{Te} is the volatility of Te relative to Sn (0 = not fractionated; 1 = completely volatile).
V_{Sb} is the volatility of Sb relative to Sn (0 = not fractionated; 1 = completely volatile).

The data and analysis given by Asryan et al. (2004) suggest that Sb will likely be present in the form Sb_2O_4 under similar conditions. They show that the sublimation of this compound is congruent, while that of the more common Sb_2O_3 is incongruent and decomposes into Sb_2O_4 upon sublimation. The total pressure above Sb_2O_3 is ~1 atm at 797 °C and would be ~0.01 atm at 697 °C. Finally, while SnO_2 is the most stable oxide at low temperature it decomposes at high temperatures and SnO is the most likely gaseous species over the temperature range of interest here (Colin et al., 1965; Lamoreaux et al., 1987). The partial pressure of this species above the solid is ~1 atm at ~2250 °C and is ~0.01 atm at ~1800 °C. These data strongly suggest that if the glass surfaces were closed to mass transfer at temperatures of approximately ~1050–1250 °C (the melting temperature of a rock with the bulk chemical composition of the fallout studied herein; Gualda et al., 2012), and if all of the main oxide forms of Sn, Sb and Te were soluble in the glass, we would expect to have essentially all of the Sn incident on the liquid present in solution, and essentially none of the Sb or Te in the limit of an ideal solution. Even with real solutions it is unlikely that a significant fraction of the Sb and Te would remain in solution. These partial pressures are thus inconsistent with the effective volatilities extracted from the analysis of the xenon isotope ratios (i.e., are inconsistent with the observation that Sb is not fractionated from Sn).

Given this result it is natural to examine the opposite limit, where the interaction of the fuel and fission products with the molten soil took place under reducing or oxygen-deficient conditions. The implication here is that the likely presence of a substantial quantity of metal in a device assembly, combined with the short time allowed for mixing with the ambient atmosphere (<3 s), prevents oxidation of the fission products to a significant extent prior to solidification of fallout. In Table 3 we present data on the partial pressures of elemental Sn, Sb, and Te. Based on these data, it appears that the results from our analysis of the xenon isotope ratios are more in accord with an oxygen-starved system (either in the fireball or upon interaction with the molten silicate droplets) than a highly-oxidizing environment. Under oxidizing or reducing conditions one infers that Sn will always behave as though it was refractory. However, contrary to the conclusions drawn from consideration of pure oxide species, the elemental vapor pressures imply that Sb will appear significantly more refractory than Te under reducing conditions. If the surface of the liquids became impervious to mass transfer at temperatures of ~1050–1250 °C, it is reasonable to expect that little or no tellurium would be found in solution.

Table 3
Volatilities of Xe precursor nuclides.

Species	T (°C) where Vp = 1 atm	T (°C) where Vp = 0.1 atm
Sn[a]	2620	1834
Sb[a]	1585	946
Te[a]	992	615
SnO[b]	2250	1800
Sb_2O_3[c]	797	697
TeO_2[d]	1080	867

[a] Cohen et al. (2003).
[b] Colin et al. (1965); Lamoreaux et al. (1987).
[c] Asryan et al. (2004).
[d] Narasimhan et al. (2005).

The time required to oxidize vaporized fission products and metals associated with a nuclear detonation depends on the mass of vaporized material, yield, and the rate at which air is entrained at the base of the buoyantly rising fireball. Our data suggest that the fireball may have remained partially oxygen-deficient, at least in isolated regions, for up to several seconds. Alternatively, it is possible that fission products were present in the fireball as oxides and then were reduced upon interaction with the silicate droplets, although the silicate melts are already in a highly oxidized state that may preclude species from donating oxygen upon collision. It is also possible that our assumptions regarding the stable oxide speciation and vapor pressure relationships of the fission products at fireball temperatures are inaccurate, and the relative volatility relationships inferred from our analysis are in fact consistent with oxidized species. However, taking the experimental data discussed above at face value, it appears that the Xe isotopes may provide constraints on the time required to draw a sufficient volume of atmospheric oxygen into the buoyantly rising fireball to oxidize fission products and metals. Clearly there is much more to probe in order to determine the conditions that prevailed in defining the characteristics of the fallout that we have studied. But it is equally clear that the analysis of xenon isotopes opens a door to an improved understanding of the mechanisms and details of fallout formation, including further insight into the characteristics of chemical fractionation. Such improved constraints on fission product chemistry and condensation, both temporally and spatially within fireball, are essential for validating and improving models of fallout formation.

5. Conclusions

Temporal constraints from short-lived Xe chronometry indicate that (1) regions of the nuclear fireball in which the fallout glasses formed cooled to temperatures below ~1200 °C within ~3 s, and/or (2) the fallout glasses were ejected from the fireball within ~3 s. Thermochemical constraints gleaned from relative volatility relationships suggest that Xe precursors may have been present in the fireball as reduced atomic species, or may have been reduced upon interaction with the silicate melts. The very short times over which Xe precursors were incorporated into these melts, coupled with the implication that Te was significantly more volatile than Sn and Sb, provides insight into the thermal and chemical environments that existed during the ~3 s required for the surfaces of the liquids to have become effectively impervious to mass transport. In particular, given the assumptions regarding the oxide speciation and vapor pressure relationships of fission products outlined above, the data appear to be inconsistent with the notion that a strongly oxidizing environment prevailed in the regions of the fireball over the timescales probed by the glassy fallout considered here.

More generally, inter-sample variations in the times of formation and relative volatilities of fissiogenic nuclides indicate fallout formation is a spatially and/or temporally heterogeneous process. We conclude that Xe isotopes can be used to quantify radionuclide fractionation arising due to both thermochemical effects and temporal variations. Xe isotope data thus represent a new approach to studying fission product chemistry and fallout formation. A salient strength of the technique is the freedom from significant corrections due to background contributions or chemical fractionation. This work highlights the importance of fundamental data on the high-temperature vapor phase behavior of fission product

elements, under both reducing and oxidizing conditions, in improving our understanding of differences in radionuclide fractionation and fallout formation.

Acknowledgements

This work performed under the auspices of the U.S. Department of Energy by Lawrence Livermore National Laboratory under Contract DE-AC52-07NA27344. We thank the U.S. Department of Energy's National Nuclear Security Administration, Office of Defense Nuclear Nonproliferation Research and Development, for financial support. Jim Delmore and two anonymous reviewers are thanked for their thoughtful and constructive reviews of the manuscript.

Appendix A. Supplementary data

Supplementary data related to this article can be found at http://dx.doi.org/10.1016/j.jenvrad.2014.06.011.

References

Adams, C., Farlow, N., Schell, W., 1960. The compositions, structures and origins of radioactive fall-out particles. Geochim. Cosmochim. Acta 18, 42–56.
Adams, C.E., O'Connor, J.D., 1957. The Nature of Individual Radioactive Particles, VI: Fallout Particles from a Tower Shot, Operation Redwing.
Asryan, N.A., Alikhanyan, A.S., Nipan, G.D., 2004. p-T-x phase diagram of the Sb-O system. Inorg. Mater. 40, 626–631.
Atkatz, D., Bragg, C., 1995. Determining the yield of the Trinity nuclear device via gamma-ray spectroscopy. Am. J. Phys. 63, 411–413.
Beck, H.L., Bouville, A., Moroz, B.E., Simon, S.L., 2010. Fallout deposition in the Marshall Islands from Bikini and Enewetak nuclear weapons tests. Health Phys. 99, 124.
Belloni, F., Himbert, J., Marzocchi, O., Romanello, V., 2011. Investigating incorporation and distribution of radionuclides in trinitite. J. Environ. Radioact. 102, 852–862.
Bellucci, J.J., Simonetti, A., 2012. Nuclear forensics: searching for nuclear device debris in trinitite-hosted inclusions. J. Radioanal. Nucl. Chem. 293, 313–319.
Bellucci, J.J., Simonetti, A., Wallace, C., Koeman, E.C., Burns, P.C., 2013a. Isotopic fingerprinting of the world's first nuclear device using post-detonation materials. Anal. Chem. 85, 4195–4198.
Bellucci, J.J., Wallace, C., Koeman, E.C., Simonetti, A., Burns, P.C., Kieser, J., Port, E., Walczak, T., 2013b. Distribution and behavior of some radionuclides associated with the Trinity nuclear test. J. Radioanal. Nucl. Chem. 295, 2049–2057.
Bunch, T.E., Hermes, R.E., Moore, A.M., Kennett, D.J., Weaver, J.C., Wittke, J.H., DeCarli, P.S., Bischoff, J.L., Hillman, G.C., Howard, G.A., 2012. Very high-temperature impact melt products as evidence for cosmic airbursts and impacts 12,900 years ago. In: Proceedings of the National Academy of Sciences, vol. 109, pp. E1903–E1912.
Carney, K.P., Finck, M.R., McGrath, C.A., Martin, L.R., Lewis, R.R., 2014. The development of radioactive glass surrogates for fallout debris. J. Radioanal. Nucl. Chem. 299, 363–372.
Cohen, Richard E., Lide, David R., Trigg, George L. (Eds.), 2003. AIP Physics Desk Reference, third ed. Springer/AIP Press, NY, ISBN 0387989730. QC61 .A37 2003.
Colin, R., Drowart, J., Verhaegen, G., 1965. Mass-spectrometric study of the vaporization of tin oxides – dissociation energy of SnO. Trans. Faraday Soc. 61, 1364–1371.
Eby, N., Hermes, R., Charnley, N., Smoliga, J.A., 2010. Trinitite: the atomic rock. Geol. Today 26, 180–185.
England, T., Rider, B., 1994. Evaluation and Compilation of Fission Yields, ENDF-349. LA-UR-94-3106.
Fahey, A., Zeissler, C., Newbury, D., Davis, J., Lindstrom, R., 2010. Postdetonation nuclear debris for attribution. In: Proceedings of the National Academy of Sciences, vol. 107, pp. 20207–20212.
Freiling, E.C., 1961. Radionuclide fractionation in bomb debris. Science 133, 1991–1998.
Gualda, G.A.R., Ghiorso, M.S., Lemons, R.V., Carley, T.L., 2012. Rhyolite-MELTS: a modified calibration of MELTS optimized for silica-rich, fluid-bearing magmatic systems. J. Petrol. 53, 875–890.
Izrael, Y.A., 2002. Radioactive fallout after nuclear explosions and accidents. Radioact. Environ. 3, 1–281.
Jessberger, E., Jordan, J., Shukolykov, Y.A., Meshik, A., Minh, D.V., 1992. In: Widespread Alien Xe and its Formation, Lunar and Planetary Institute Science Conference Abstracts, p. 615.
Joint Working Group of the American Physical Society and the American Association for the Advancement of Science, 2010. Nuclear Forensics: Role, State of the Art, Program Needs.
Kawahara, F.K., Freiling, E.C., Bunney, L.R., Crocker, G.R., 1980. Fallout from Nuclear Cratering Shot Danny Boy: I – Radiochemical Analysis and Some Physical Observations on Selected Samples.
Lamoreaux, R.H., Hildenbrand, D.L., Brewer, L., 1987. High-temperature vaporization behavior of oxides II. Oxides of Be, Mg, Ca, Sr, Ba, B, Al, Ga, in, Tl, Si, Ge, Sn, Pb, Zn, Cd, and Hg. J. Phys. Chem. Ref. Data 16, 419.
Mackin, J., Zigman, P., Love, D., MacDonald, D., Sam, D., 1960. Radiochemical analysis of individual fall-out particles. J. Inorg. Nucl. Chem. 15, 20–36.
Meshik, A., Pravdivtseva, O., Hohenberg, C., 2005. Fission xenon in trinitites. Meteorit. Planet. Sci. Suppl. 40, 5321.
Miller, C.F., 1960. A Theory of Formation of Fallout from Land-surface Nuclear Detonations and Decay of the Fission Products. Naval Radiological Defense Laboratory, San Francisco, CA.
Narasimhan, T.S., Baba, M.S., Viswanathan, R., 2005. Vaporization behavior of TeO2 (s): a quantitative vaporization – Knudsen effusion mass spectrometric study. Thermochim. Acta 427, 137–147.
National Research Council of the National Academies – Committee on Nuclear Forensics, 2010. Nuclear Forensics, a Capability at Risk.
Parekh, P.P., Semkow, T.M., Torres, M.A., Haines, D.K., Cooper, J.M., Rosenberg, P.M., Kitto, M.E., 2006. Radioactivity in trinitite six decades later. J. Environ. Radioact. 85, 103–120.
Pittauerova, D., Kolb, W.M., Rosenstiel, J.C., Fischer, H.W., 2010. Radioactivity in trinitite – a review and new measurements. In: Proceedings of Third European IRPA Congress, June, pp. 14–16.
Renne, P., Cassata, W., Morgan, L., 2009. The isotopic composition of atmospheric argon and $^{40}Ar/^{39}Ar$ geochronology: time for a change? Quat. Geochronol. 4, 288–298.
Schlauf, D., Siemon, K., Weber, R., Esterlund, R., Molzahn, D., Patzelt, P., 1997. Trinitite redux: comment on "determining the yield of the Trinity nuclear device via gamma-ray spectroscopy" by David Atkatz and Christopher Bragg [Am. J. Phys. (5), 411–413 (1995)]. Am. J. Phys. 65, 1110.
Shibata, T., Takahashi, E., Matsuda, J.-I., 1998. Solubility of neon, argon, krypton, and xenon in binary and ternary silicate systems: a new view on noble gas solubility. Geochim. Cosmochim. Acta 62, 1241–1253.
Stewart, K., 1956. The condensation of a vapour to an assembly of droplets or particles. Trans. Faraday Soc. 52, 161–173.